A regime diagram for ocean geostrophic turbulence

A. Klocker[a]*, D. P. Marshall[b], S. R. Keating[c], P. L. Read[b]

[a]*Institute for Marine and Antarctic Studies, University of Tasmania, Hobart, Tasmania, Australia*
[b]*Department of Physics, University of Oxford, Oxford, UK*
[c]*School of Mathematics and Statistics, University of New South Wales, Sydney, New South Wales, Australia*

*Correspondence to: A. Klocker, Institute for Marine and Antarctic Studies, University of Tasmania, 20 Castray Esplanade, Battery Point, TAS 7004, Australia.
E-mail: andreas.klocker@utas.edu.au

A two-dimensional regime diagram for geostrophic turbulence in the ocean is constructed by plotting observation-based estimates of the nondimensional eddy radius and unsuppressed mixing length against a nonlinearity parameter equal to the ratio of the root-mean square eddy velocity and baroclinic Rossby phase speed. For weak nonlinearity, as found in the tropics, the mixing length mostly corresponds to the stability threshold for baroclinic instability whereas the eddy radius corresponds to the Rhines scale; it is suggested that this mismatch is indicative of the inverse energy cascade that occurs at low latitudes in the ocean and the zonal elongation of eddies. At larger values of nonlinearity, as found at mid- and high-latitudes, the eddy length scales are much shorter than the stability threshold, within a factor of 2.5 of the Rossby deformation radius.

Key Words: geostrophic turbulence, mesoscale eddies, eddy mixing, Rhines scale, baroclinic instability, mixing length

Received . . .

1. Introduction

The ocean is a turbulent fluid with transient motions on a plethora of spatial and temporal scales. The large-scale circulation is dominated by the turbulent geostrophic eddy field, with an eddy spatial scale that correlates with the Rossby deformation radius (Stammer 1997). Interactions between the turbulent geostrophic eddies and the large-scale flow have a profound impact on the circulation and stratification of the global ocean (e.g., Rhines and Young 1982; Gent *et al.* 1995; Wolfe and Cessi 2010; Munday *et al.* 2013), yet will need to be parameterized in many numerical ocean models for the foreseeable future (e.g., Fox-Kemper *et al.* 2013).

One common approach to eddy parameterization is to employ mixing length arguments to derive an eddy diffusivity proportional to an eddy velocity multiplied by an eddy length scale. This approach has been used to develop full eddy closures for both the atmosphere and the ocean (e.g., Bretherton (1966); Green (1970); Stone (1972); Held and Larichev (1996); Visbeck *et al.* (1997); Eden and Greatbach (2008); Marshall and Adcroft (2010)) but exactly what sets this eddy length scale remains an active topic of research.

The most comprehensive study of eddy length scales has been carried out by Tulloch *et al.* (2011) who found that observed eddy length scales exceed the energy injection scale at all latitudes, with the latter occurring at scales larger than the deformation radius at high latitudes, and at scales smaller than the deformation radius at low latitudes. Recently, Klocker and Abernathey (2014) (henceforth KA14) have used two measures of the eddy length scale in order to estimate eddy diffusivities. The first is the eddy "radius" of Chelton *et al.* (2011). The second is a mixing length scale inferred from a passive tracer field, modified to remove the kinematic suppression of mixing by background mean flow (Ferrari and Nikurashin 2010; Klocker *et al.* 2012).

The aim of this short contribution is to introduce and physically interpret a *regime diagram* of geostrophic turbulence in the ocean in which these two observation-based estimates of eddy length scales correspond to different dynamical *regime transitions*. The manuscript is structured as follows. In section 2, we summarize the method of data analysis and describe the regime diagram which allows us to interpret observation-based eddy length scales and compare these length scales with scaling theories. In section 3, we physically interpret the observation-based eddy length scales in terms of dynamical regime transitions. A brief concluding discussion is given in section 4.

2. The regime diagram

The regime diagram (Fig. 1) is constructed by plotting measures of a nonlinearity parameter, defined as the ratio of the root-mean squared eddy velocity and the Rossby phase speed (Chelton *et al.* 2011), against eddy length scales, normalized by the baroclinic deformation radius. To calculate these variables we use nearly two decades worth of satellite measurements of sea-surface height (SSH). We focus on a region in the Pacific Ocean, ranging from 60^oS to 50^oN and 180^oW to 130^oW, which covers a wide parameter space of the regime diagram. Eddy properties can be thought of as predominantly latitude dependent in this region, enabling us to use zonal averages of flow properties.

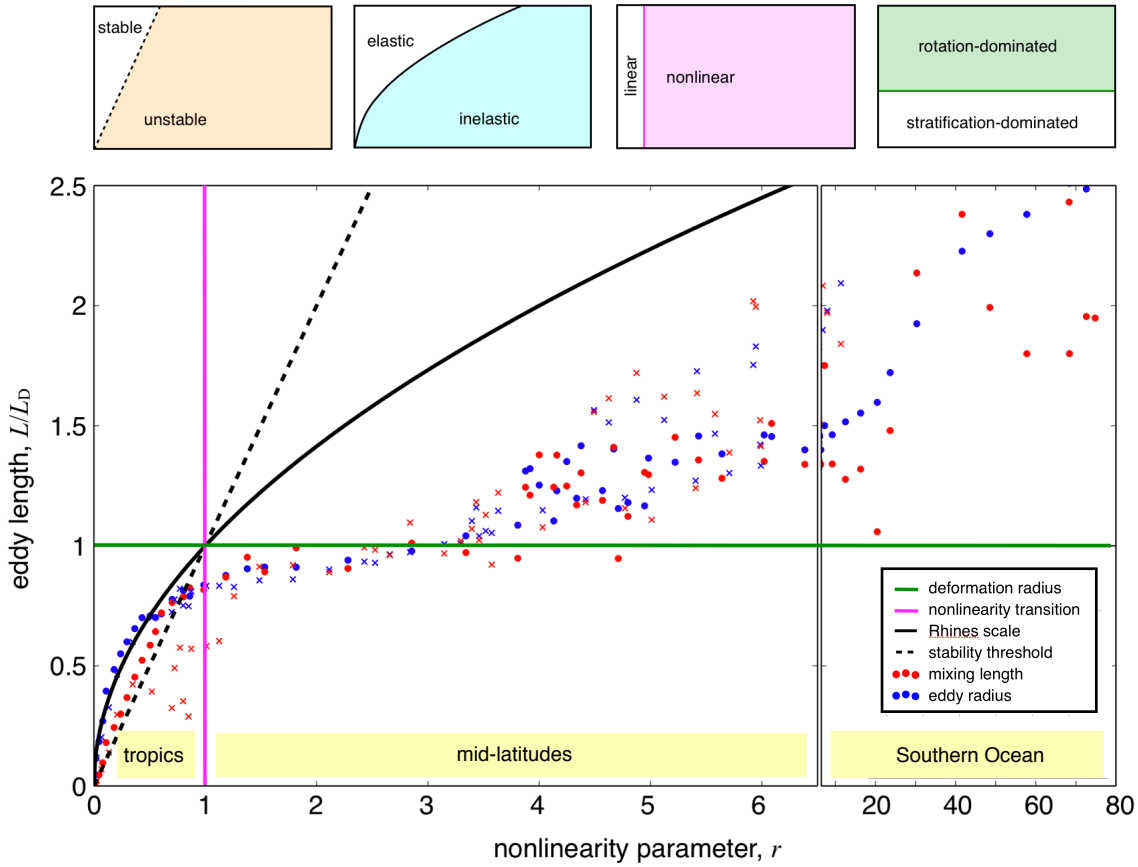

Figure 1. The regime diagram for ocean geostrophic turbulence. The axes correspond to the nonlinearity parameter, r, and the nondimensional eddy length scales, L/L_D. The blue symbols correspond to the nondimensional eddy radius and the red symbols to the nondimensional mixing length; dots are for the southern hemisphere and crosses for the northern hemisphere. The dashed black line is the stability threshold, the solid black line is the Rhines scale, the magenta line is the nonlinearity transition, and the green line is the deformation radius. These lines represent regime transitions from one dynamical regime to another as indicated in the upper panels. For further details, see the main text.

The data used here are the same as in KA14 where the authors showed a close relationship between observed eddy length scales and eddy diffusivities when mean flow effects are accounted for. This paper now adds a layer of interpretation in terms of explaining the behaviour of these eddy length scales across various regime transitions of geostrophic turbulence.

The nonlinearity parameter, represented by the x-axis in the regime diagram, is defined following Chelton *et al.* (2011) as

$$r = \frac{U_{\mathrm{eddy}}}{c}, \tag{1}$$

where U_{eddy} is the root-mean squared eddy velocity, $c = \beta L_D^2$ is the long Rossby wave speed at which mesoscale eddies propagate westward (Cushman-Roisin *et al.* 1990; Chelton *et al.* 2007), β is the meridional gradient of the Coriolis parameter and L_D the deformation radius. Here U_{eddy} is calculated using SSH-derived geostrophic velocities as an anomaly of the long-term mean. Since the calculation of the deformation radius requires knowledge of the stratification, we employ values for L_D from Tulloch *et al.* (2009) who used an ocean state estimate (Forget 2010), i.e., an ocean model strongly constrained to observations, to calculate the Rossby wave speed in the long-wave limit. Note that these methods of estimating U_{eddy} and c are both different to those used by Chelton *et al.* (2007, 2011).

Note that we do not include the effects of background mean flow in the definition of the long Rossby wave speed, c. To the extent that the mean flow has the same modal structure as the Rossby wave mode under consideration, the Doppler shifting of the Rossby wave is exactly cancelled by the modification of the background potential vorticity gradient by the associated buoyancy gradients through thermal wind balance. This is known as the 'non-Doppler effect' (Held 1983; Colin de Verdiere and Tailleux 2005; Samelson 2010). There may be some residual Doppler effect by other modes (Killworth *et al.* 1997; Dewar 1998; de Szoeke and Chelton 1999) but this is not considered here.

The normalized eddy length scales, represented by the y-axis in the regime diagram, can be written as L/L_D. Here L is either the observed eddy radius, $L = R_{obs}$, or the eddy mixing length, $L = L_{mix}$.

Eddy radii R_{obs} are calculated using an eddy tracking algorithm based on the same SSH field (Chelton *et al.* 2011), with the eddy radius being defined as the radius of a circle of area equal to that enclosed by contours of SSH within the eddy around which the contour-average speed is maximum. R_{obs}/L_D is shown as red dots and crosses in Fig. 1, with dots representing the southern hemisphere and crosses representing the northern hemisphere. It is worth noting here that whereas the altimeter has limited spatial resolution, it has been shown that the dominant eddy length scales for both velocity and heat flux estimated from the altimeter are very closely related to the eddy radii estimated by Chelton *et al.* (2011), and are very similar to eddy length scales in high-resolution ocean models (Abernathey and Wortham 2015), suggesting that the resolution of the altimeter may be sufficient for estimating the eddy length scales discussed here.

Mixing length arguments state that eddy diffusivities are proportional to the root-mean squared eddy velocity U_{eddy} times a mixing length L_{mix} (Taylor 1915; Prandtl 1925), where the mixing length depends on both eddy properties and mean flow properties (Ferrari and Nikurashin 2010; Klocker *et al.* 2012). KA14 then used geostrophic velocities derived from satellite measurements, and by systematically varying the mean flow in this velocity field derived an eddy mixing length which is only dependent on eddy properties, i.e. with all mean flow effects

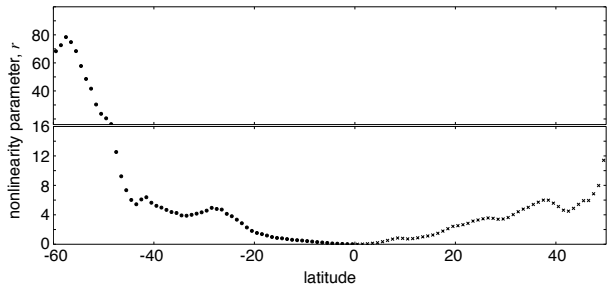

Figure 2. Variation of the nonlinearity parameter, r, with latitude. Dots correspond to the southern hemisphere and crosses to the northern hemisphere, as in Fig. 1.

removed. This length scale is often called the unsuppressed mixing length. Since here we are interested in the efficiency of eddies to transport tracers, and not the mean flow, we will use these eddy mixing lengths in the regime diagram, where L_{mix}/L_D is shown as blue dots and crosses in Fig. 1.

To understand the geographical distribution of the nondimensional variables in the regime diagram we distinguish tropics, mid-latitudes and the Southern Ocean in the panels on the bottom of Fig. 1. We also plot the nonlinearity parameter (Eq. (1)) versus latitude in Fig. 2. Small values (less than 1) are found in the tropics, with larger values (greater than 1) at mid- and high-latitudes, where the change between tropics and mid-latitudes (coinciding with values equal 1) is known as the critical latitude, further described in the next setion; the maximum values are found in the Southern Ocean.

3. Regime transitions

We now come to the main purpose of this manuscript, which is to interpret the observation-based eddy length scales on the regime diagram in terms of pertinent regime transition lines. These regime transitions refer to boundaries along which there is change in dynamical behavior. This change may be abrupt, e.g., through the crossing of a stability threshold, or gradual, through the dominance of different physical processes to either side of the transition.

3.1. *Transition from linear to nonlinear dynamics*

Flow regimes can be categorized as predominantly linear or nonlinear depending on whether or not an eddy can be regarded as a linear wave disturbance propagating through a nearly stationary flow. These regimes are distinguished using the *nonlinearity parameter* defined in Eq. (1) (Chelton *et al.* 2011).

If $r > 1$, the rotational velocity of the eddy, U_{eddy}, exceeds its translational velocity, roughly approximated by the long Rossby wave speed* , c (Chelton *et al.* 2007). Transforming coordinates into the co-moving frame results in closed streamlines within the eddy, i.e., an inner core that is able to advect tracers, and an outer ring that is capable of stirring tracers (Early *et al.* 2011). If $r \leq 1$, the translational velocity of the eddy exceeds its rotational velocity and transforming coordinates into the co-moving frame does not result in closed streamlines within the eddy. The latitude corresponding to $r = 1$ is termed the *critical latitude* (Theiss 2004) and can be used to distinguish regions of isotropic turbulence ($r > 1$) from regions with anisotropic turbulence ($r < 1$) in which turbulence induces alternating (baroclinic) zonal jets (Okuno and Masuda 2003; Theiss 2004).

In the regime diagram (Fig. 1) the change from linear to nonlinear dynamics is represented on the x-axis, with the line at the value of 1 (the magenta line in Fig. 1) being the regime transition line from linear dynamics (for values less than 1) to nonlinear dynamics (for values greater than 1).

The eddy length scales exhibit very different behavior to either side of the transition, with the two measures of eddy length departing from each other in the linear regime, but being broadly indistinguishable from each other in the nonlinear regime. In each of the linear and nonlinear regimes, a distinct functional variation of the eddy length scale with the nonlinearity parameter is obtained. These are discussed in more detail in the following sections.

3.2. *Transition from rotation- to stratification-dominated flow*

Geophysical turbulence is strongly influenced by rotation and stable stratification with small Rossby number, $\mathrm{Ro} = U/fL$, and Froude number, $\mathrm{Fr} = U/c_{grav} = U/fL_D$, where U is a characteristic velocity scale, f is the Coriolis parameter, L is a characteristic eddy length scale and $c_{grav} = fL_D$ is the speed of an internal gravity wave. The relative importance of rotation and stratification is quantified by the *Burger number*,

$$Bu = \frac{\mathrm{Ro}^2}{\mathrm{Fr}^2} = \frac{L_D^2}{L^2}. \tag{2}$$

In rotation-dominated flow, typical length scales are larger than the deformation radius, whereas in stratification-dominated flow, typical length scales are smaller than the deformation radius. In energetically favoured scales of motion in stably-stratified flow, the Burger number is O(1) leading to length scales of O(L_D) (Read 2001).

In the regime diagram (Fig. 1) the influence of rotation and stratification is represented on the y-axis, with the line at the value of 1 (the green line in Fig. 1), i.e. length scales equal to the deformation radius, being the regime transition line between rotation-dominated flow (for values greater than 1) to stratification-dominated flow (for values less than 1). This transition from rotation- to stratification-dominated flow ocurs at about $r \approx 3$.

Note that the eddy scale at which the transition occurs from linear to nonlinear dynamics coincides roughly with the transition from stratification- to rotation-dominated flow (more precisely this occurs at $L/L_D \approx 0.8$). In the nonlinear regime, the observed eddy length scales exceed the deformation radius by only a modest amount (typically a factor between 1 and 2, with values of 2.5 in the Southern Ocean). We also observe a much greater spread in both eddy length scales in the rotation-dominated regime in which $L/L_D > 1$.

3.3. *Transition from stable to unstable flow*

Mesoscale eddies derive their energy primarily from baroclinic instability. Using the original argument for baroclinic adjustment (Stone 1978), based on the condition for marginal criticality for baroclinic zonal flow in the two-layer quasigeostrophic (QG) model (Phillips 1951), the *criticality parameter* can be written (Held and Larichev 1996) as

$$\xi = \frac{\overline{U}_{\mathrm{thermal}}}{c} = \frac{\overline{U}_{\mathrm{thermal}}}{\beta L_D^2}, \tag{3}$$

where $\overline{U}_{\mathrm{thermal}}$ is the mean zonal velocity from the thermal wind relation (i.e. baroclinic shear) and $\xi > 1$ is the criterion or baroclinic instability in an inviscid flow. Equivalently, using the thermal wind relation, this criticality parameter can be expressed as a critical value of the meridional temperature gradient (Stone 1978).

*This approximation neglects the advection of eddies by the depth-averaged mean flow, as described in Klocker and Marshall (2014).

In supercritical mean states, $\xi > 1$, the flow is baroclinically unstable leading to turbulent flow in the form of mesoscale eddies, possibly with an inverse energy cascade from the scale of the instability towards the Rhines scale through nonlinear eddy-eddy interactions. These mesoscale eddies then enhance the meridional eddy flux of temperature, bringing the meridional temperature gradient towards its critical value – a process that has been termed *baroclinic adjustment* (Stone 1978).

The criticality parameter ξ is closely related to the deformation radius, the Rhines scale and the nonlinearity parameter. To see this, we use the result from Held and Larichev (1996) that for $\xi > 1$ the root-mean squared eddy velocity is related to the mean thermal wind by

$$U_{\text{eddy}} \approx \frac{L}{L_D} \overline{U}_{\text{thermal}}, \tag{4}$$

derived by scaling the eddy potential vorticity flux and the implied eddy energy production, and assuming an inverse cascade. Thus the condition for baroclinic instability in this limit can be rewritten

$$\frac{L}{L_D} \lesssim r, \tag{5}$$

i.e., mesoscale eddies can only grow if their nondimensional length scale is less than the nonlinearity parameter (see the Appendix for a more detailed derivation). In the following we use the term *stability threshold* to describe this transition between baroclinic unstable and stable flow, i.e., the state of marginal criticality.

In the regime diagram (Fig. 1) the stability threshold is shown as a black dashed line, with flow above this line being baroclinically stable and below this line being baroclinically unstable.

For $r < 1$ the unsuppressed eddy mixing length scale lies close to the stability threshold over much of the data points with some smaller values in the northern hemisphere, possibly due to the larger amplitude of Tropical Instability Waves in the northern hemisphere (Chelton and Schlax 2000). However, for $r > 1$ the stability threshold lies within the rotation-dominated regime in which motion along the rotation axis, and hence release of available potential energy, is inhibited by rotational constraints; instead, the energy release occurs on scales comparable to the deformation radius consistent with baroclinic instability theory (Charney 1948; Eady 1949; Phillips 1951). Tulloch *et al.* (2011) calculated the most unstable length scales for the global ocean and finds that these slightly exceed the deformation radius at mid- and high latitudes, consistent with Fig. 1 for $r > 1$.

3.4. *Transition from weak to strong Rossby elasticity*

Just as stable stratification inhibits vertical motion, so the variation of the Coriolis parameter with latitude inhibits meridional motion. The Rossby restoring force arises through considering the vorticity dynamics acting on a line of fluid parcels and gives rise to westward propagation. See a standard text such as Vallis (2006) for discussion of the Rossby wave mechanism and Marshall and Pillar (2011) for a physical interpretation of the Rossby restoring force.

The efficiency of the Rossby restoring force or *Rossby elasticity* (Dritschel and McIntyre 2008) is quantified by considering the ratio of planetary vorticity variations and relative vorticity anomalies, with the transition occurring at the *Rhines scale*,

$$L_{\text{Rhines}} = \sqrt{\frac{U_{\text{eddy}}}{\beta}} \tag{6}$$

(Rhines 1975). In the regime diagram (Fig. 1) the transition from Rossby elasticity being inelastic to being elastic is represented by the thick black line.

Below this transition, Rossby elasticity is insufficient to prevent turbulent mixing across latitude circles, whereas above this transition, strong Rossby elasticity prevents significant meridional displacements and Rossby waves dominate (although see Sukoriansky *et al.* 2007, for a more careful discussion). An alternative physical interpretation is that closed potential vorticity contours can occur on scales shorter than the Rhines scale, but not above.

A logical extension of the Rhines scale, developed for barotropic flow, is to allow a finite deformation radius (Okuno and Masuda 2003; Theiss 2006). Using the same arguments that lead to the Rhines scale, this then leads to its baroclinic counterpart,

$$L^{bci}_{\text{Rhines}} = \sqrt{\frac{U_{\text{eddy}}}{\beta} \frac{1}{1-r}}. \tag{7}$$

Hence for nonlinear dynamics ($r > 1$), Rossby elasticity is always insufficient to prevent turbulent mixing across latitude circles.

For $r < 1$, we find that the two nondimensional eddy lengths diverge from each other, with the mixing length coinciding with the stability threshold, but the eddy radius coinciding with the Rhines scale, possibly inducing alternating zonal flows in these regions (Rhines 1975; Theiss 2004).

For $r > 1$, the observed eddy scales coincide with each other and are much shorter than the Rhines scale. This becomes apparent when rewriting the nonlinearity parameter, using Eq. (7), as

$$r = \left(\frac{L_{\text{Rhines}}}{L_D} \right)^2 \tag{8}$$

and recalling that the observed eddy length scales slightly exceed the deformation scale in this regime (see Fig 1). Consistent with Tulloch *et al.* (2011), the observed eddy scales are approximately 25% smaller than the Rhines scale. In this regime Tulloch *et al.* (2011) identify a slight mismatch between the energy injection scale and observed eddy length scale which they suggest might be indicative of a limited inverse cascade.

3.5. *Turbulent β scale*

Finally, we discuss the relation of our results to the length scale formed from the turbulent energy flux or eddy generation rate, ϵ, and the meridional gradient in the Coriolis parameter (Vallis and Maltrud 1993),

$$L_\beta = \frac{\epsilon^{1/5}}{\beta^{3/5}}. \tag{9}$$

This length scale corresponds most closely to the scale at which β-plane turbulence becomes anisotropic and is always smaller than the Rhines scale.

The eddy generation rate ϵ, using quasi-geostrophic theory and assuming a zonal flow, can be written as

$$\epsilon = \langle U \overline{u'q'} \rangle \approx UK\beta, \tag{10}$$

where $U = U_{thermal}$ and K is the eddy PV diffusivity.

To test how the turbulent β scale relates to the observed eddy length scales, we first rewrite the nondimensional turbulent β scale as

$$\frac{L_\beta}{L_D} = \frac{\epsilon^{1/5}}{\beta^{1/10}\, c^{1/2}}, \tag{11}$$

similar to the ratio $\tilde{\beta}$ of Smith (2004), where we have used $c = \beta L_D^2$. The advantage of (11) is that the nondimensional turbulent β scale depends weakly on both ϵ and β: the variation in $\beta^{1/10}$

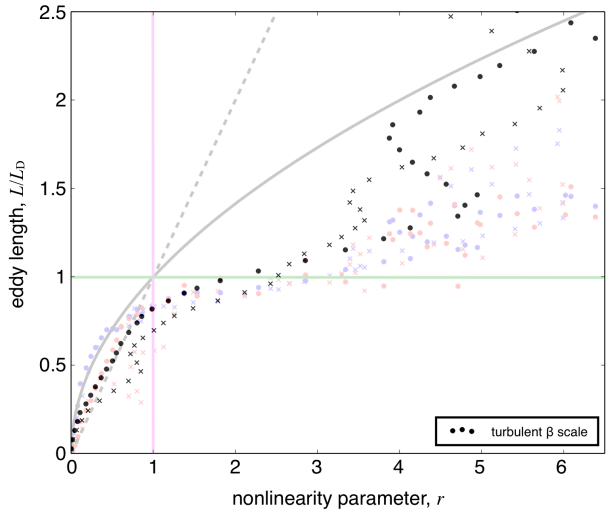

Figure 3. The nondimensional turbulent β scale, L_β/L_D, with $\epsilon = 4 \times 10^{-9}\,\mathrm{m^2 s^{-3}}$, plotted on the same regime diagram as in Fig. 1 for $r \leq 6.5$. Black dots are for the northern hemisphere and black crosses are for the southern hemisphere. The data and regime transitions lines from Fig. 1 are shown in faint in the background.

is less than 7% between the equator and 60°, and the variation in the $\epsilon^{1/5}$ due to an order of magnitude (factor of 10) uncertainty is by a factor of just 1.6. Thus the variation of L_β/L_D in (11) is dominated by the variation of the inverse square-root of the Rossby wave speed, c.

We now plot this nondimensional turbulent β scale in Fig. 3, using a constant eddy generation rate of $\epsilon = 4 \times 10^{-9} m^2 s^{-3}$, which is in the range of ϵ values estimated from satellite observations and high-resolution ocean models by (Arbic *et al.* 2014, their Figs. 10 and 11), and chosen to give the best fit to the observation-based data. This shows that the theoretical prediction (11) captures much of the observed variation of the eddy length scale with latitude, in particular when the latter is identified as the unsuppressed mixing length. Nevertheless, similar agreement is achieved using a constant L_β, suggesting that most of the variability of the eddy length scales with the nonlinearity parameter is set by the deformation scale. On the other hand, observed values of the turbulent energy flux ϵ lead to the correct order of magnitude of eddy length scales, suggesting a role for ϵ in setting eddy length scales and agreeing with the conjecture that the diffusion coefficient of the poleward heat transport depends on the turbulent energy flux (Held and Larichev 1996; Held 1999; Lapeyre and Held 2003).

4. Concluding remarks

In this paper, we have introduced a two-dimensional regime diagram for geostrophic turbulence in the ocean. The axes correspond to the nonlinearity parameter and the eddy length scale, normalized by the deformation radius. Two observation-based measures of the eddy length scale are plotted on the diagram, corresponding to the eddy radius and the eddy mixing length (with suppression effects of the mean flow removed).

We have shown that the observed eddy length scales coincide with different regime transitions on the diagram. In the linear regime, obtained in the tropics, the eddy radius corresponds to the Rhines scale whereas the eddy mixing length corresponds to the stability threshold. In the nonlinear regime, both the eddy radius and eddy mixing length correspond to (a multiple just over unity of) the deformation radius. These results are consistent with previous studies, e.g., Tulloch *et al.* (2011) and references therein.

One limitation of this study is none of the theories considered here are viable candidates for explaining eddy length scales at higher latitudes, where missing effects such as drag and topography are likely to play a significant role and which could explain the spread of eddy length scales at these latitudes. A further limitation is that we have been unable to fully distinguish between the barotropic and baroclinic components of the flow, for which the properties of the turbulent cascade differ (e.g., Salmon 1998). These issues should be addressed in future studies.

The eddy length scale is an important quantity for constructing parameterizations of geostrophic eddies. Specifically mixing length arguments are used to express the eddy diffusivity as proportional to an eddy velocity multiplied by an eddy length scale. This regime diagram can now be used to interpret these observed eddy length scales and, by extension, the physical mechanisms underlying mixing lengths in eddy parameterizations. The variation of the eddy radius on the regime diagram is broadly consistent with the simple proposal of Eden and Greatbach (2008) that the eddy length scale is given by the minimum of the Rhines scale and the deformation radius. However, as noted by Fox-Kemper *et al.* (2013), small differences between the observed eddy length scale and the deformation radius (up to 2.5 in the nonlinear regime) can make a large difference when it comes to practical implementation of a parameterization. More future work is necessary to understand the role of the turbulent β length scale in setting eddy length scales, which itself is largely set by the turbulent energy flux ϵ. This dependency would agree with the conjecture that the diffusion coefficient of the poleward heat transport depends on the turbulent energy flux ϵ (Held and Larichev 1996; Held 1999; Lapeyre and Held 2003; Sukoriansky *et al.* 2009).

An interesting avenue for future research would be to plot the observed eddy radii and mixing lengths for flows in other rotating, stratified fluids such as the atmospheres of the Earth and gas giants, to determine whether the regimes we find in the ocean occur more widely. Work in this direction by Cho and Polvani (1996) has shown that using a simple shallow-water model and the observed values of radius, rotation rate, average wind velocity, and mean layer thickness, all of which are used in the calculation of the deformation radius and the Rhines scale, it is possible to reproduce observations of the flow on Jupiter, Saturn, Uranus and Neptune. Additionally, Theiss (2006) showed that when taking into account a finite deformation radius and a zonal mean flow, the nonlinearity parameter is very successful in distinguishing regions with alternating zonal flows and storms on Jupiter. These results therefore suggest that the regime diagram introduced here might be more universal.

5. Appendix: Derivation of the stability threshold for baroclinic instability

We have defined the following nondimensional parameters: the nonlinearity parameter

$$r = \frac{U_{\mathrm{eddy}}}{\beta L_D^2}, \tag{12}$$

and the Burger number

$$Bu^{-1/2} = \frac{L}{L_D} \tag{13}$$

where U_{eddy} and L are the velocity and length scale of the eddy, L_D is the deformation scale, and β is the planetary vorticity gradient.

Held and Larichev (1996) derived a scaling argument for baroclinic instability based upon the criticality parameter

$$\xi = \frac{U_{\mathrm{thermal}}}{\beta L_D^2}, \tag{14}$$

where $U_{\rm thermal}$ is the thermal wind velocity (baroclinic shear). The condition for baroclinic instability is $\xi > 1$. Note that all of the dimensional parameters appearing in the definition of ξ refer to the large scale flow, that is, $\xi > 1$ is a condition for baroclinic instability of the thermal wind shear. Now, when the flow is unstable, Held and Larichev (1996) found that the following scaling relations hold,

$$\frac{U_{\rm eddy}}{U_{\rm thermal}} \approx \xi, \qquad \frac{L_D}{L} \approx \xi^{-1}, \qquad \text{when} \qquad \xi > 1. \tag{15}$$

[These relations are actually quoted in the abstract of Held and Larichev, 1996.] It is straightforward to rearrange this so that

$$U_{\rm eddy} \approx \frac{L}{L_D} U_{\rm thermal}, \qquad \text{when} \qquad \xi > 1. \tag{16}$$

This is Eq. (4) in the paper. This relation provides a scaling relation between the eddy velocity and the thermal wind velocity *when the flow is baroclinically unstable*.

Eq. (5) in the paper is then derived by rewriting the criticality parameter in terms of the nonlinearity parameter $r = U_{\rm eddy}/\beta L_D^2$,

$$\xi = \frac{U_{\rm thermal}}{\beta L_D^2} = r \frac{U_{\rm thermal}}{U_{\rm eddy}}. \tag{17}$$

When the flow is baroclinically unstable we can make use of the Held and Larichev scaling for $U_{\rm eddy}$,

$$\xi \approx r \frac{L_D}{L} > 1. \tag{18}$$

Finally, this is rearranged to give Eq. (5)

$$r > \frac{L}{L_D}. \tag{19}$$

Note again that this relation is valid only when $\xi > 1$, i.e., when the large-scale flow is unstable.

Acknowledgement

The authors thank Ross Tulloch for providing data and Dudley Chelton, Boris Gaplerin and Michael McIntyre for useful discussions which helped to improve this manuscript. This work started during a visit of AK to the University of Oxford supported by an Australian Bicentennial Fellowship. AK was supported by a Australian Research Council Discovery Early Career Researcher Award (DE140100076). SRK was suppported by a UNSW Faculty Research Grant. DPM was partially supported by the Oxford Martin School.

References

Abernathey R, Wortham C. 2015. Phase speed cross spectra of eddy heat fluxes in the eastern Pacific. J. Phys. Oceanogr., submitted.

Arbic BK, Müller M, Richman JG, Shriver JF, Morton AJ, Scott RB, Sérazin G, Penduff T. 2014. Geostrophic turbulence in the frequency-wavenumber domain: Eddy-driven low-frequency variability. *J. Phys. Oceanogr.* **44**: 2025–2069.

Bretherton FP. 1966. Critical layer instability in baroclinic flows. *Quart. J. Roy. Meteor. Soc.* **92**: 325–334.

Charney JG. 1948. On the scale of atmospheric motions. *Geofys. Publ. Oslo* **17**: 1–17.

Chelton DB, Schlax MG. 2000. Satellite microwave SST observations of transequatorial tropical instability waves. *Geophys. Res. Lett.* **27**: 1239–1242.

Chelton DB, Schlax MG, Samelson RM. 2011. Global observations of nonlinear mesoscale eddies. *Prog. Oceanogr.* **91**: 167–216.

Chelton DB, Schlax MG, Samelson RM, de Szoeke RA. 2007. Global observations of large oceanic eddies. *Geophys. Res. Lett.* **34**: L15 606, doi:10.1029/2007GL030 812.

Cho JYK, Polvani M. 1996. The morphogenesis of bands and zonal winds in the atmosphere on the giant outer planets. *Science* **273**: 335–337.

Colin de Verdiere A, Tailleux R. 2005. The interaction of a baroclinic mean flow with long rossby waves. *J. Phys. Oceanogr.* **35**: 865–879.

Cushman-Roisin B, Chassignet EP, Tang B. 1990. Westward motion of mesoscale eddies. *J. Phys. Oceanogr.* **20**: 758 768.

de Szoeke RA, Chelton DB. 1999. The modification of long planetary waves by homogeneous potential vorticity layers. *J. Phys. Oceanogr.* **29**: 500–511.

Dewar WK. 1998. On too fast baroclinic planetary waves in the general circulation. *J. Phys. Oceanogr.* **28**: 1739–1758.

Dritschel DG, McIntyre ME. 2008. Multiple jets as PV staircases: The Phillips effect and the resilience of eddy-transport barriers. *J. Atmos. Sci.* **65**: 855–874.

Eady ET. 1949. Long waves and cyclone waves. *Tellus* **1**: 33–52.

Early JJ, Samelson RM, Chelton DB. 2011. The evolution and propagation of quasigeostrophic ocean eddies. *J. Phys. Oceanogr.* **41**: 1535–1555.

Eden C, Greatbach RJ. 2008. Towards a mesoscale eddy closure. *Ocean Modell.* **20**: 223–239.

Ferrari R, Nikurashin M. 2010. Suppression of eddy diffusivity across jets in the Southern Ocean. *J. Phys. Oceanogr.* **40**: 1501–1519.

Forget G. 2010. Mapping ocean observations in a dynamical framework: A 2004-06 ocean atlas. *J. Phys. Oceanogr.* **40**: 1201–1221.

Fox-Kemper B, Lumpkin R, Bryan FO. 2013. Ocean circulation and climate: A 21st century perspective. In: *Lateral Transport in the Ocean Interior*, Siedler G, Griffies SM, Gould J, Church JA (eds), Elsevier, pp. 185–209.

Gent PR, Willebrand J, McDougall TJ, McWilliams JC. 1995. Parameterizing eddy-induced tracer transports in ocean circulation models. *J. Phys. Oceanogr.* **25**: 463–474.

Green JSA. 1970. Transfer properties of the large-scale eddies and the general circulation of the atmosphere. *Quart. J. Roy. Meteor. Soc.* **96**: 157–185.

Held IM. 1983. Stationary and quasi-stationary eddies in the extratropical troposphere: theory. In: *Large-Scale Dynamical Processes in the Atmosphere*, Hoskins BJ, Pearce RP (eds), Academic Press, pp. 127–168.

Held IM. 1999. The macroturbulence of the troposphere. *Tellus* **51A**: 59–70.

Held IM, Larichev VD. 1996. A scaling theory for horizontally homogeneous, baroclinically unstable flow on a beta plane. *J. Atmos. Sci.* **53**: 946–953.

Killworth PD, CHelton DB, deSzoeke RA. 1997. The speed of observed and theoretical long extratropical planetary waves. *J. Phys. Oceanogr.* **27**: 1946–1966.

Klocker A, Abernathey R. 2014. Global patterns of mesoscale eddy properties and diffusivities. *J. Phys. Oceanogr.* **44**: 1030–1046.

Klocker A, Ferrari R, LaCasce JH. 2012. Estimating suppression of eddy mixing by mean flows. *J. Phys. Oceanogr.* **42**: 1566–1576.

Klocker A, Marshall DP. 2014. Advection of baroclinic eddies by depth mean flow. *Geophys. Res. Lett.* **41**: 3517–3521.

Lapeyre G, Held IM. 2003. Diffusivity, kinetic energy dissipation, and closure theories for the poleward eddy heat flux. *J. Atmos. Sci.* **60**: 2907–2916.

Marshall DP, Adcroft AJ. 2010. Parameterization of ocean eddies: Potential vorticity mixing, energetics and Arnold's first stability theorem. *Ocean Modell.* **32**: 188–204.

Marshall DP, Pillar HR. 2011. Momentum balance of the wind-driven and meridional overturning circulation. *J. Phys. Oceanogr.* **41**: 960–978.

Munday DR, Johnson HL, Marshall DP. 2013. Eddy saturation of equilibrated circumpolar currents. *J. Phys. Oceanogr.* **43**: 507–532.

Okuno A, Masuda A. 2003. Effect of horizontal divergence on the geostrophic turbulence on a beta-plane: Suppression of the Rhines effect. *Phys. Fluids.* **15**: 56–65.

Phillips NA. 1951. A simple three-dimensional model for the study of large-scale extratropical flow patterns. *J. Meteor.* **8**: 381–393.

Prandtl L. 1925. Bericht über Untersuchungen zur ausgebildeten Turbulenz. *Z. Angew. Math. Mech.* **5**: 136–139.

Read P. 2001. Transition to geostrophic turbulence in the laboratory, and as a paradigm in atmospheres and oceans. *Survey Geophys.* **22**: 265–317.

Rhines P, Young W. 1982. Homogenization of potential vorticity in planetary gyres **122**: 347–367.

Rhines PW. 1975. Waves and turbulence on a β-plane. *J. Fluid Mech.* **69**: 417–443.

Salmon R. 1998. *Lectures on geophysical fluid dynamics*. Oxford University Press.

Samelson R. 2010. An effective-β vector for linear planetary waves on a weak mean flow. *Ocean Modell.* **32**: 170–174.

Smith KS. 2004. A local model for planetary atmospheres forced by small-scale convection. *J. Atmos. Sci.* **61**: 1420–1433.

Stammer D. 1997. Global characteristics of ocean variability estimated from regional TOPEX/POSEIDON altimeter measurements. *J. Phys. Oceanogr.* **27**: 1743–1769.

Stone PH. 1972. A simplified radiative-dynamical model for the static stability of rotating atmospheres. *J. Atmos. Sci.* **29**: 405–418.

Stone PH. 1978. Baroclinic adjustment. *J. Atmos. Sci.* **35**: 561–571.

Sukoriansky S, Dikovskaya N, Galperin B. 2009. Transport of momentum and scalar in turbulent flows with anisotropic dispersive waves. *Geophys. Res. Lett.* **36**: L14 609, DOI: 10.1029/2009GL038 632.

Sukoriansky S, Galperin B, Dikovskaya N. 2007. On the arrest of inverse energy cascade and the Rhines scale. *J. Atmos. Sci.* **64**: 3312–3327.

Taylor GI. 1915. Eddy motion in the atmosphere. *Philosophical Transactions of the Royal Society A* **215**: 1–26.

Theiss J. 2004. Equatorward energy cascade, critical latitude, and the predominance of cyclonic vortices in geostrophic turbulence. *J. Phys. Oceanogr.* **34**: 1663–1678.

Theiss J. 2006. A generalized Rhines effect and storms on Jupiter. *Geophys. Res. Lett.* **33**: doi:10.1029/2005GL025 379.

Tulloch R, Marshall J, Hill C, Smith KS. 2011. Scales, growth rates and spectral fluxes of baroclinic instability in the ocean. *J. Phys. Oceanogr.* **41**: 1057–1076.

Tulloch R, Marshall J, Smith KS. 2009. Interpretation of the propagation of surface altimetric observations in terms of planetary waves and geostrophic turbulence. *J. Geophys. Res.* **114**: C02 005, doi:10.1029/2008JC005 055.

Vallis GK. 2006. *Atmospheric and oceanic fluid dynamics*. Cambridge University Press.

Vallis GK, Maltrud ME. 1993. Generation of mean flows and jets on a beta plane over topography. *J. Phys. Oceanogr.* **23**: 1346–1362.

Visbeck M, Marshall J, Haine T. 1997. Specifcation of eddy transfer coefficients in coarse-resolution ocean circulation models. *J. Phys. Oceanogr.* **27**: 381–403.

Wolfe CL, Cessi P. 2010. What sets the strength of the middepth stratification and overturning circulation in eddying ocean models? *J. Phys. Oceanogr.* **40**: 1520–1538.

